Mechanistic Roles of Tyrosine Phosphorylation in Reversible Amyloids, Autoinhibition, and Endosomal Membrane Association of ALIX

Ruben D. Elias, Bhargavi Ramaraju, and Lalit Deshmukh*

*Corresponding author. Email: ldeshmukh@ucsd.edu

This PDF file includes:

Figs. S1 to S14
Tables S1 to S2
Table S3 (Separate excel file that contains all peptides and PTMs identified by LC-MS/MS)
References (1 to 10)

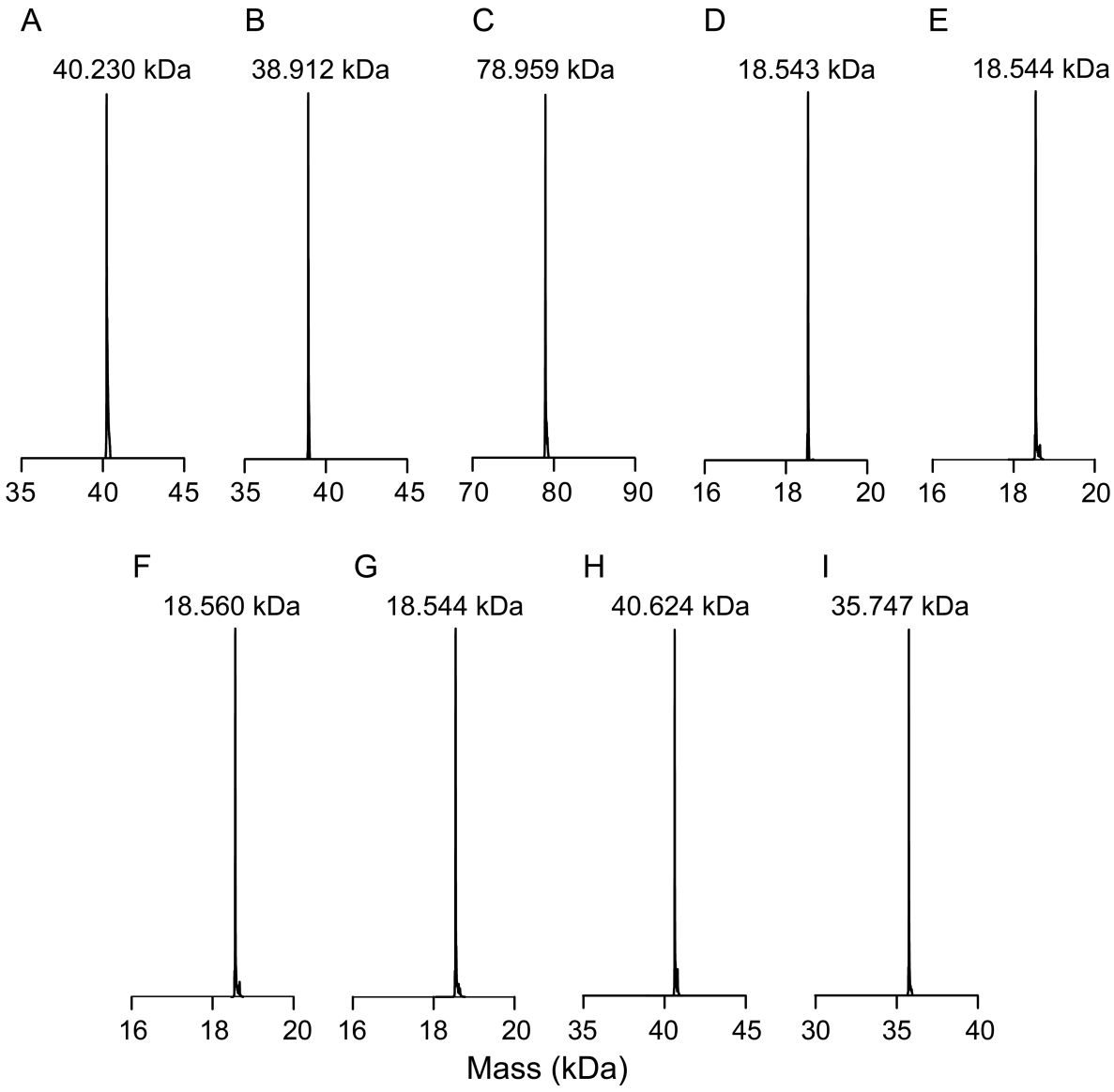

Fig. S1. LC-ESI-TOFMS analysis of recombinant protein constructs used in current study. (**A**) Bro1, calculated mass: 40.231 kDa; (**B**) V, calculated mass: 38.912 kDa; (**C**) Bro1-V, calculated mass: 78.957 kDa; (**D**) $PRD^{Strep}_{703\text{-}868}$, calculated mass: 18.544 kDa; (**E**) $PRD^{Strep}_{703\text{-}868}$-S712C,C813S, calculated mass: 18.544 kDa; (**F**) $PRD^{Strep}_{703\text{-}868}$-A756C,C813S, calculated mass: 18.560 kDa; (**G**) $PRD^{Strep}_{703\text{-}868}$-S863C,C813S, calculated mass: 18.544 kDa; (**H**) MBP-E38C, calculated mass: 40.624 kDa; (**I**) catalytic domain of PTP1B, calculated mass: 35.747 kDa. The masses of the following two constructs, $PRD^{Strep}_{703\text{-}800}$ and full-length Src, are reported in our previous work (1).

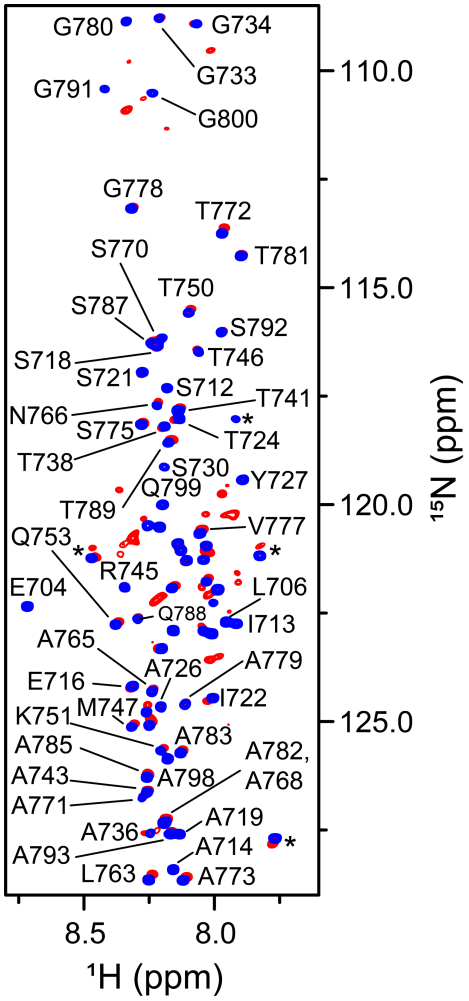

Fig. S2. NMR analysis of hyperphosphorylated $PRD^{Strep}_{703-868}$. Overlay of expanded regions of the ^{1}H-^{15}N TROSY-HSQC correlation spectra of $PRD^{Strep}_{703-800}$ (blue) and hyperphosphorylated $PRD^{Strep}_{703-868}$ (red); 100 µM each. Some of the isolated cross-peaks of $PRD^{Strep}_{703-800}$ are labelled. The backbone resonance assignments of $PRD^{Strep}_{703-800}$ are taken from our previous work (1), biological magnetic resonance bank (BMRB) accession no. 28111. The cross-peaks corresponding to the C-terminal strep tag (WSHPQFEK) of $PRD^{Strep}_{703-800}$ are marked with asterisks. Backbone resonance assignments of hyperphosphorylated $PRD^{Strep}_{703-868}$ were not feasible owing to the complexity and the heterogeneity of its phosphorylation pattern. All data were acquired at a spectrometer ^{1}H frequency of 800 MHz at 30 °C. Buffer conditions were as follows: 20 mM sodium phosphate, pH 6.5, 50 mM NaCl, 1 mM TCEP, and 2 mM EDTA.

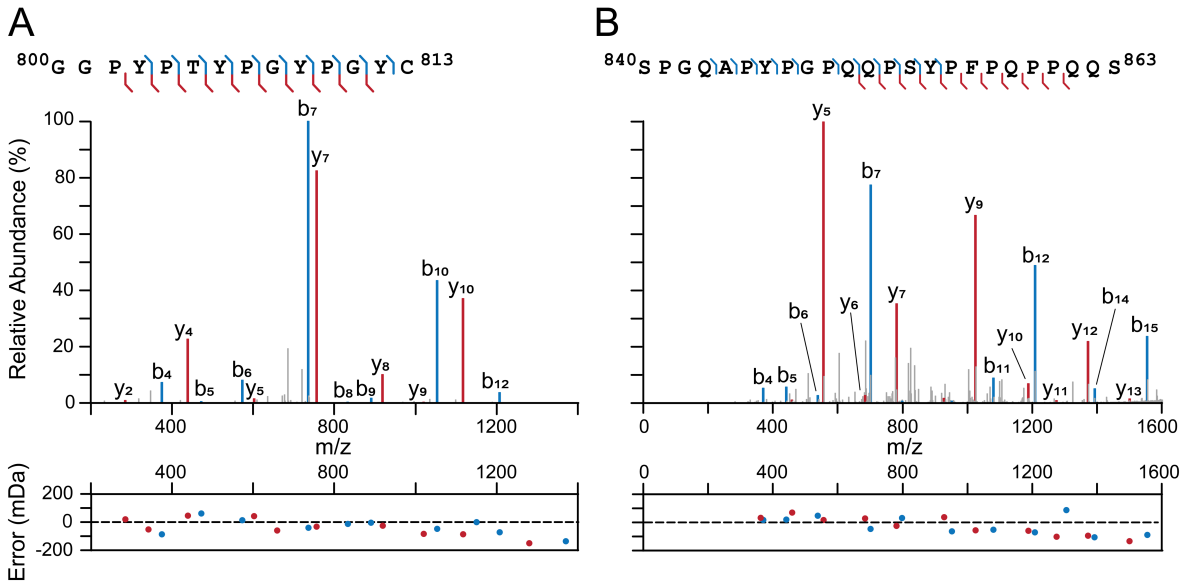

Fig. S3. LC-MS/MS analysis of PK-digestion of $PRD^{Strep}_{703-868}$ fibrils. (**A-B**) Panels show the assignment of collision-induced dissociation (CID) fragment ions to the peptide primary sequence according to the standard nomenclature (2). The b_n and y_n ions are denoted by the blue and red brackets, respectively. Residuals (observed spectral position minus calculated m/z) for each fragment ion peak are plotted below the panels. The figure was formatted using IPSA (3). Also see Table S2 for the list of search parameters used for analyses and Table S3 for the list of all peptides that were identified.

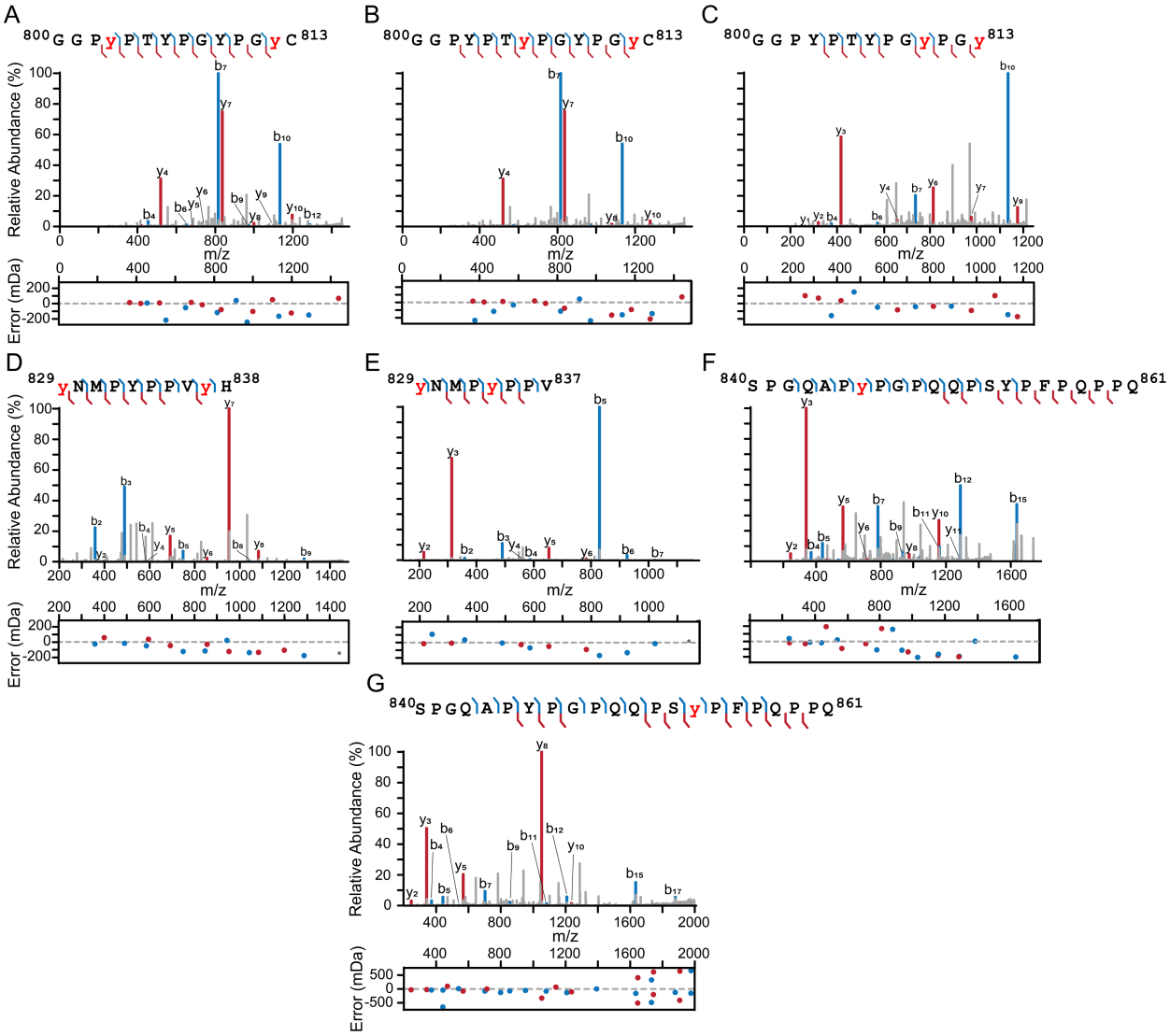

Fig. S4. LC-MS/MS analysis of PK digestion of hyperphosphorylated $PRD^{Strep}_{703-868}$. (**A-F**) Panels show the assignment of collision-induced dissociation (CID) fragment ions to the peptide primary sequence. The b_n and y_n ions are denoted by the blue and red brackets, respectively. Phosphorylated tyrosine residues are denoted in red. Residuals (observed spectral position minus calculated m/z) for each fragment ion peak are plotted below the panels. The figure was formatted using IPSA (3). Also see Table S2 for the list of search parameters used for analyses and Table S3 for the list of all peptides that were identified. The above results are in excellent agreement with our previous results of LC-MS/MS analysis of chymotrypsin digested hyperphosphorylated $PRD_{800-868}$ (1).

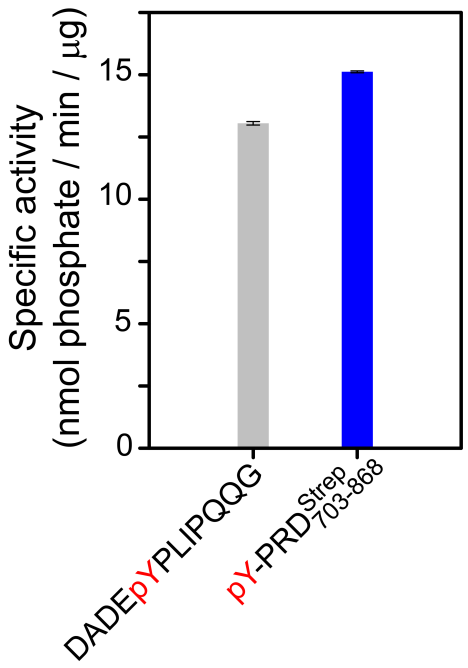

Fig. S5. Quantification of PTP1B activity. The activity of the catalytic domain of recombinant PTP1B was measured using a malachite green phosphate detection assay kit (R&D systems, Inc). Data are expressed as means ± s.e.m. of three replicates. The specific activity against the control tyrosine phosphatase substrate (4); primary sequence: DADEpYPLIPQQG, where pY is phosphorylated tyrosine, is similar to the value reported by R&D systems, Inc for their commercially available PTP1B (>15 nmol/min/µg). Buffer and experimental conditions were as follows: 20 mM HEPES, pH 7.5, 1 mM DTT, 1 mM EDTA, and 30°C.

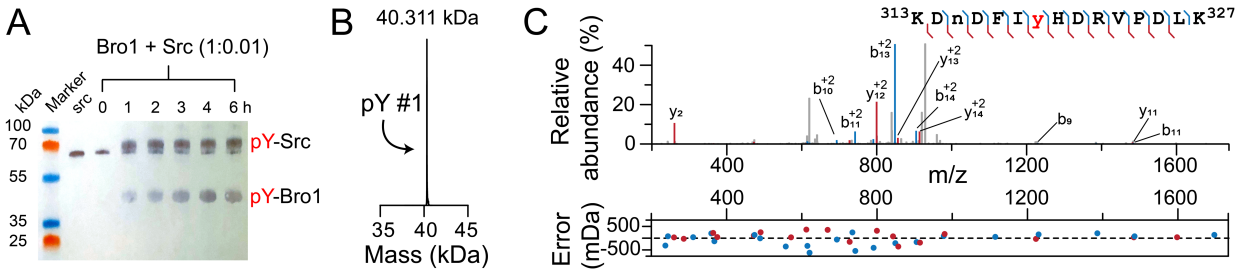

Fig. S6. Analyses of Src-mediated in vitro phosphorylation of Bro1. (**A**) Time course of Src-mediated in vitro phosphorylation of Bro1 by western blotting. The concentration of Bro1 was 50 µM; the number in parenthesis represent the molar ratio of Bro1 to Src. (**B**) LC-ESI-TOFMS and (**C**) LC-MS/MS analyses of phosphorylated Bro1 revealed that Bro1 is monophosphorylated by Src at residue 319 (note that Bro1 carries 12 native tyrosine residues; cf. Fig 3C; main text). For panel C, residuals (observed spectral position minus calculated m/z) for each fragment ion peak are plotted below the panel. The phosphorylated tyrosine residue (Y319) is denoted in red. The figure was formatted using IPSA (3). Also see Table S2 for the list of search parameters used for analyses and Table S3 for the list of all peptides that were identified. Buffer and experimental conditions were as follows: 50 mM Tris, pH 7.5, 1 mM ATP, 5 mM $MgCl_2$, 0.5 mM EDTA, 2 mM DTT, and 30 °C.

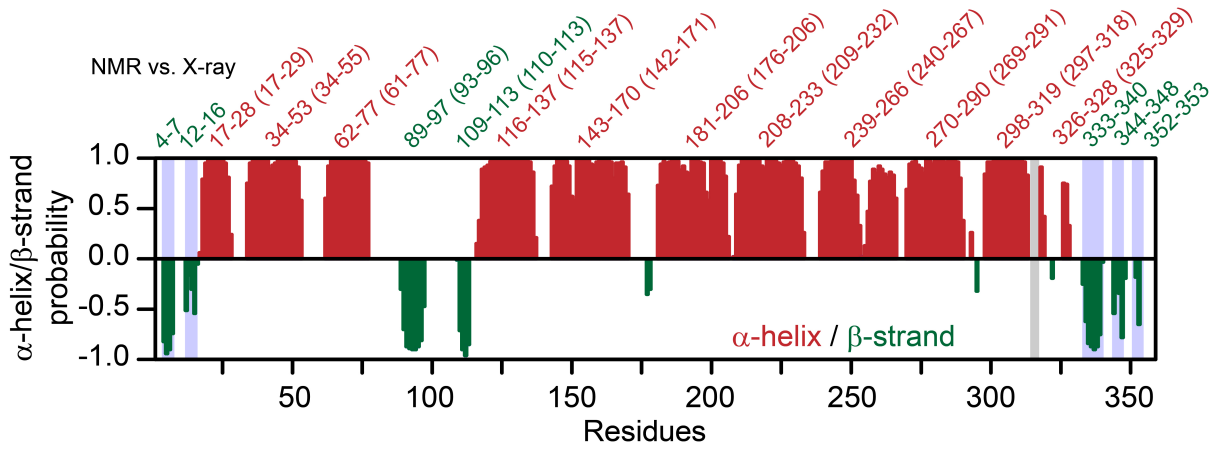

Fig. S7. NMR and X-ray derived secondary structure elements of Bro1. Secondary structure probability, α helix in red and β strand in green, derived from the backbone chemical shifts (^{13}Cα, ^{13}Cβ, ^{13}C′, ^{15}N, and $^{1}H_N$) of Bro1 using TALOS-N (5). The numbers on the top of the panel represent motifs constituting the corresponding secondary structure elements; the numbers in parenthesis are the corresponding motifs obtained from the coordinates of the X-ray structure of Bro1, Protein Data Bank (PDB) entry 5WA1 (6). Note that in contrast to X-ray, NMR chemical shifts predicted ordered strand conformations for several residues of the extreme N- and C-termini, specifically residues 4-7, 12-16, 333-340, 344-348, and 352-353 (marked in blue semi-transparent rectangles; only predictions with probability greater than 0.5 are highlighted). Semi-transparent gray rectangles mark missing predictions for residues 314-317 that could not be assigned unambiguously. Note that the low helical probability of residues 253-256 is due to the lack of availability of backbone carbon chemical shifts in that region.

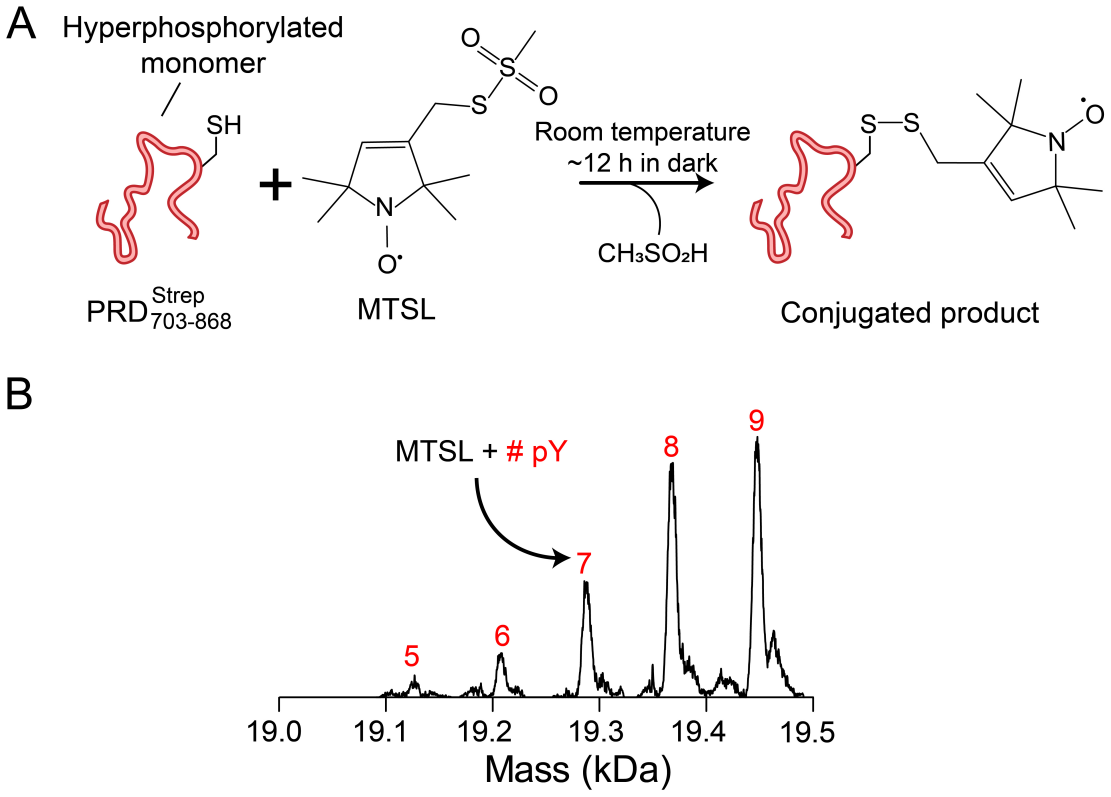

Fig. S8. Site-specific spin labeling of hyperphosphorylated $PRD^{Strep}_{703-868}$ with MTSL. (**A**) Schematic of the conjugation reaction between hyperphosphorylated $PRD^{Strep}_{703-868}$ and nitroxide spin label, MTSL. (**B**) LC-ESI-TOFMS analysis of MTSL-labeled hyperphosphorylated $PRD^{Strep}_{703-868}$. Each peak in the deconvoluted spectrum represents a conjugated product carrying one MTSL moiety; the numbers in red represent the number of phosphorylated tyrosine residues (see Table S1 for additional details).

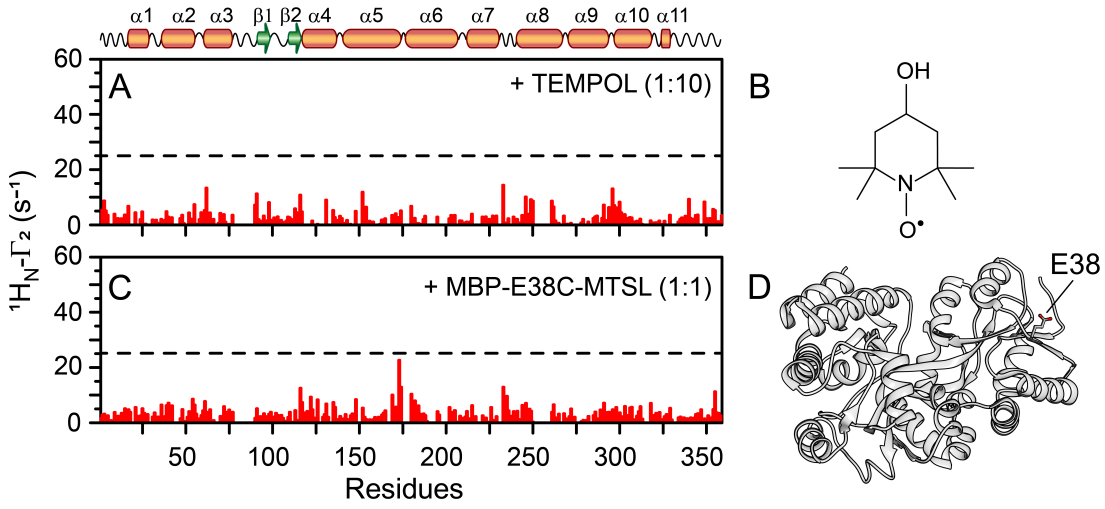

Fig. S9. Intermolecular PRE controls. Negative PRE controls (red vertical bars) are provided by the intermolecular PRE profiles observed on $^{15}N/^{2}H$-labeled Bro1 upon addition of (**A**) water soluble TEMPOL; the structure of TEMPOL is shown in panel **B**, and (**C**) apo-maltose binding protein (MBP-E38C) conjugated to a paramagnetic MTSL probe. Secondary structure elements of Bro1 are indicated above the panels. A few small solvent PREs with ^1H_N-Γ_2 values in the range of 5–10 s^{-1} are observed with TEMPOL owing to random collisions at solvent-exposed, surface accessible sites of Bro1. All PREs observed with either TEMPOL or MBP-E38C-MTSL are much smaller than those observed with hyperphosphorylated $PRD^{Strep}_{703\text{-}868}$ labeled with MTSL at site C813 (cf. Fig. 6B, top right, main text). The concentration of Bro1 was 200 μM. The numbers in parenthesis represent the molar ratios of Bro1 to TEMPOL / Bro1 to MTSL-tagged MBP-E38C. Buffer conditions were as follows: 20 mM sodium phosphate, pH 6.5, 50 mM NaCl, and 2 mM EDTA. All data were acquired at a spectrometer 1H frequency of 800 MHz at 30 °C using a two-time point method (7,8). (**D**) Ribbon representation of wild-type open form of apo MBP; Protein Data Bank (PDB) entry: 1FQA (9). Residue E38, located on the surface of MBP, is shown in stick representation.

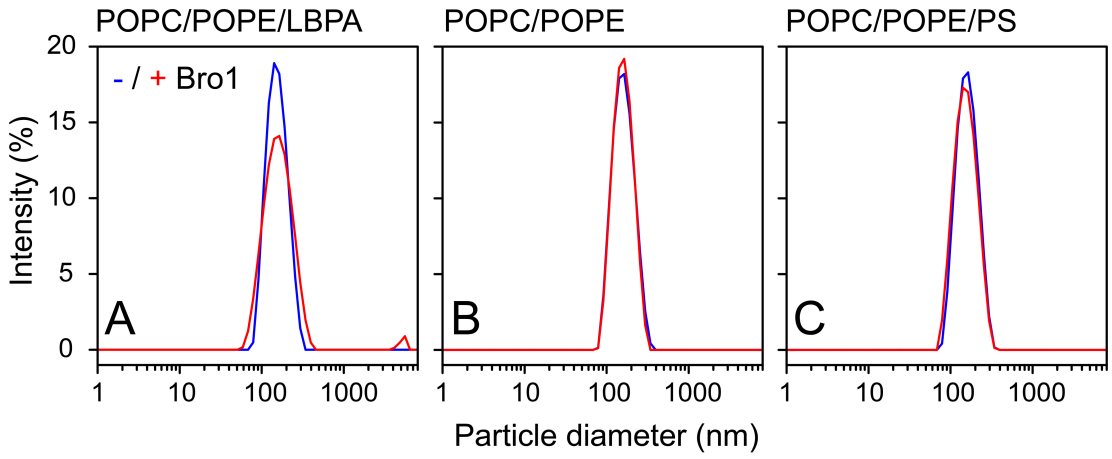

Fig. S10. Characterization of the size distribution of lipid vesicles by DLS. The following lipid vesicle compositions were used for DLS analyses, namely (**A**) negatively charged POPC/POPE/LBPA (5.5:3:1.5); (**B**) zwitterionic POPC/POPE (7:3); and (**C**) negatively charged, POPC/POPE/POPS (5.5:3:1.5); the numbers in parenthesis represent molar ratios of phospholipids. DLS measurements were carried out on 25 µM vesicles, in the absence (blue) and the presence of Bro1 (red); protein to lipid ratio of 1:1. The mean diameters of POPC/POPE/LBPA vesicles were ~150 and ~140 nm, in the absence and presence of Bro1, respectively. Zwitterionic POPC/POPE vesicles were ~150 and ~140 nm in diameter, in the absence and presence of Bro1, respectively. POPC/POPE/POPS vesicles were ~150 and ~130 nm in diameter, in the absence and presence of Bro1, respectively. Note that the POPC/POPE/LBPA vesicles revealed the presence of a small fraction of very large aggregates (>1 µm) in the presence of Bro1, indicating a likely structural rearrangement induced by Bro1 in these vesicles resulting in the formation of larger assemblies.

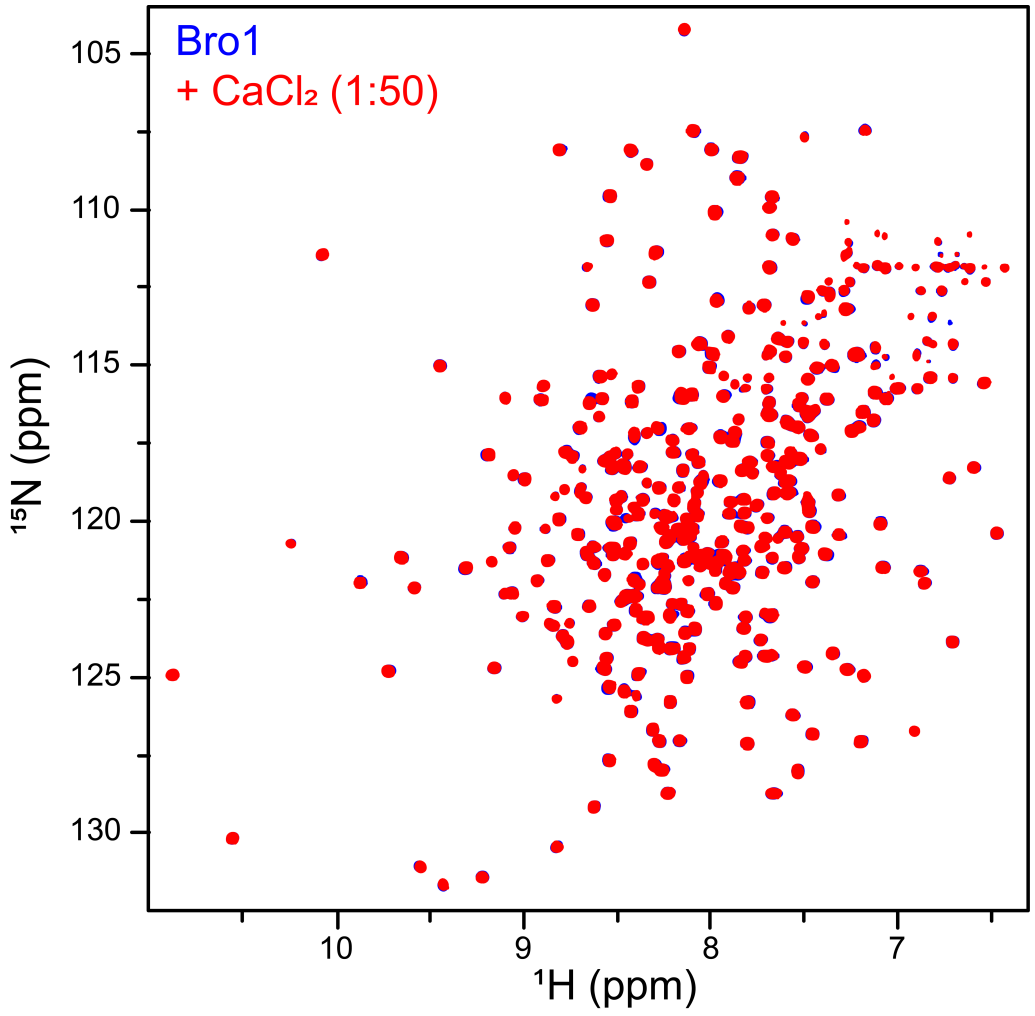

Fig. S11. NMR analysis of the lack of interactions between Bro1 and calcium. Overlay of expanded regions of ^{1}H-^{15}N TROSY-HSQC spectra of Bro1, in the absence (blue) and presence of molar excess of $CaCl_2$ (red), revealed negligible chemical shift perturbations and cross-peak attenuation. Due to the incompatibility of phosphate buffer with polyvalent cations (10), experiments were carried out in the following buffer at 30 °C, 20 mM MES, pH 6.5, 50 mM NaCl, and 1mM TCEP.

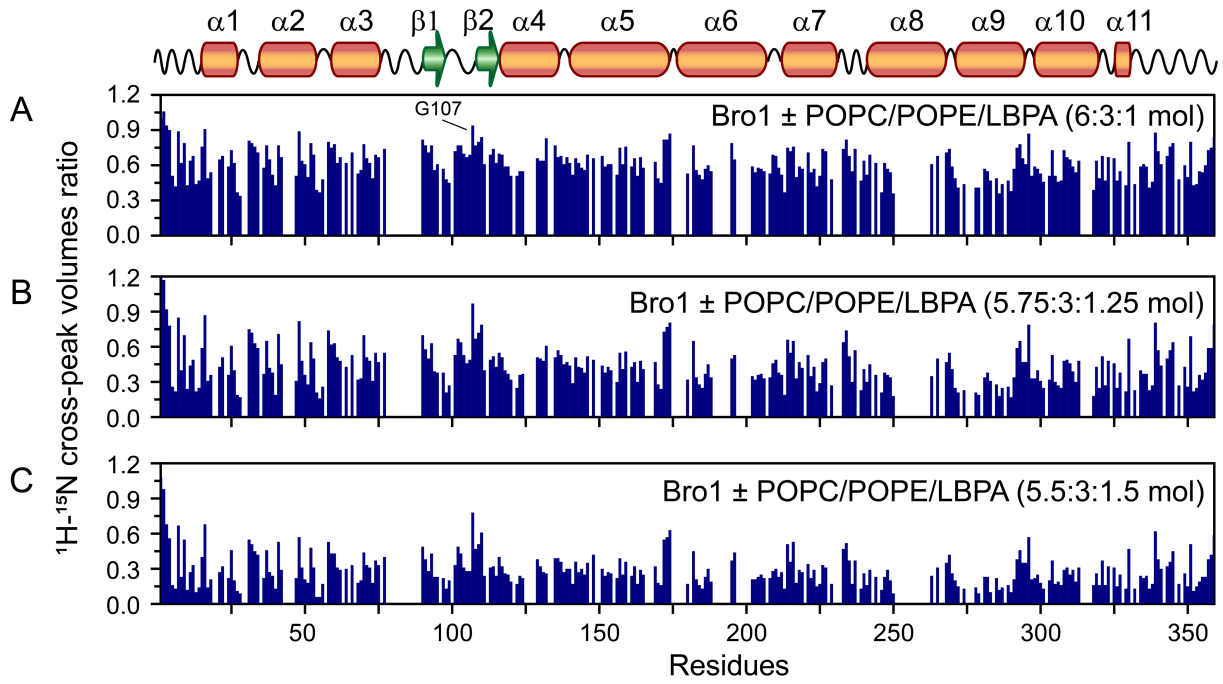

Fig. S12. NMR analyses of the association of Bro1 with LBPA-enriched lipid vesicles. The panels represent ratios of ^{1}H-^{15}N cross-peak volumes of Bro1 in the presence of LBPA-enriched lipid vesicles as compared to free Bro1. The following three vesicle compositions were used: POPC/POPE/LBPA molar ratios of (**A**) 6:3:1, (**B**) 5.75:3:1.25, and (**C**) 5.5:3:1.5. G107 of the flexible extended loop that remains relatively less affected in the presence of lipid particles is marked. All data were acquired at a spectrometer ^{1}H frequency of 800 MHz at 30 °C. Buffer conditions were as follows: 20 mM sodium phosphate, pH 6.5, 50 mM NaCl, 1 mM TCEP, and 2 mM EDTA. The concentration of $^{2}H/^{15}N$ labeled Bro1 was 100 μM with a protein to lipid molar ratio of 1:30.

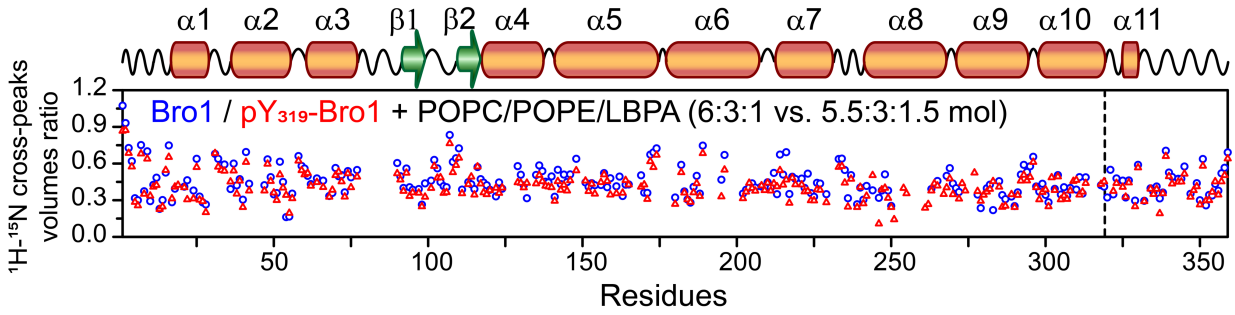

Fig. S13. Comparison of the association between non- and phosphorylated Bro1 and LBPA-enriched lipid vesicles. Comparison of the reduction in $^{1}H_{N}/^{15}N$ cross-peak volumes of $^{2}H/^{15}N$-labeled 100 μM non-phosphorylated (blue circles) and phosphorylated (red triangles) Bro1 in the presence of POPC/POPE/LBPA vesicles; protein to lipid molar ratio 1:30. The ratios of cross-peak volumes were obtained by recording two ^{1}H-^{15}N TROSY-HSQC correlation spectra of non- and –phosphorylated Bro1 (one at a time) in the presence of vesicles containing increasing amounts of LBPA; the following vesicle compositions were used: POPC/POPE/LBPA molar ratios of 6:3:1 and 5.5:3:1.5. The location of Y319 is indicated by a vertical dashed line. All data were acquired at a spectrometer ^{1}H frequency of 800 MHz at 30 °C. Buffer conditions were as follows: 20 mM sodium phosphate, pH 6.5, 50 mM NaCl, 1 mM TCEP, and 2 mM EDTA.

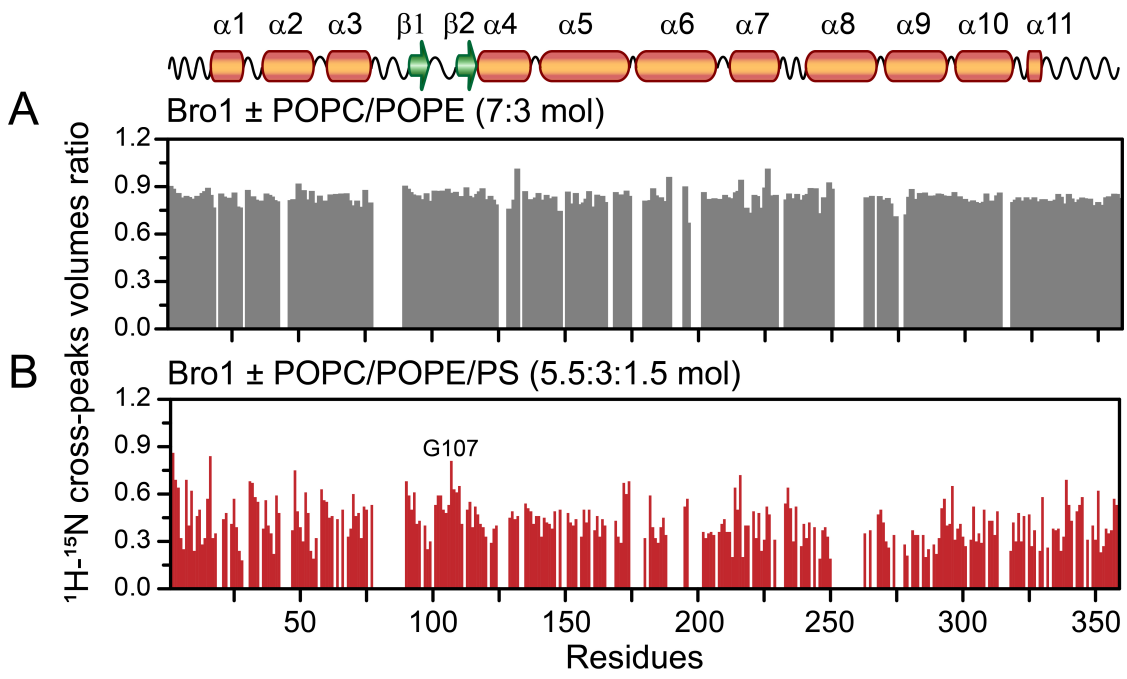

Fig. S14. Changes in $^{1}H_N/^{15}N$ cross-peak volumes of Bro1 on addition of zwitterionic and negatively charged lipid vesicles. (**A**) No significant reductions were observed in cross-peak volumes of Bro1 in the presence of zwitterionic POPC/POPE (molar ratio of 7:3) vesicles, indicative of the lack of interactions between Bro1 and zwitterionic lipid particles. (**B**) Several regions of Bro1 showed a significant reduction in cross-peak volumes on the addition of negatively charged POPC/POPE/POPS vesicles (molar ratio of 5.5:3:1.5). All data were acquired at a spectrometer ^{1}H frequency of 800 MHz at 30 °C. Buffer conditions were as follows: 20 mM sodium phosphate, pH 6.5, 50 mM NaCl, 1 mM TCEP, and 2 mM EDTA. The concentration of $^{2}H/^{15}N$ labeled Bro1 was 100 μM with a protein to lipid molar ratio of 1:30.

Table S1. LC-ESI-TOFMS analysis of Src-mediated hyperphosphorylation of $PRD^{Strep}_{703-868}$ and MTSL spin labeling of hyperphosphorylated $PRD^{Strep}_{703-868}$.[a,b]

#pY	Src + $PRD^{Strep}_{703-868}$[c,d,e]			pY - $PRD^{Strep}_{703-868}$ + MTSL[f,g]		
	Experimental	Calculated	Difference	Experimental	Calculated	Difference
1	NA	18,624	–	NA	18,808	–
2	NA	18,704	–	NA	18,888	–
3	NA	18,784	–	NA	18,968	–
4	NA	18,864	–	NA	19,048	–
5	NA	18,944	–	19,127	19,128	-1
6	19,024	19,024	0	19,208	19,208	0
7	19,104	19,104	0	19,286	19,288	-2
8	19,184	19,184	0	19,369	19,368	1
9	19,264	19,264	0	19,448	19,448	0
10	19,344	19,344	0	NA	19,528	–

a. All masses are in daltons.

b. $PRD^{Strep}_{703-868}$ contains 15 tyrosine residues (calculated mass: 18,544 Da; cf. Fig. S1D).

c. Each phosphorylated tyrosine residue accounts for an additional 80 daltons.

d. $PRD^{Strep}_{703-868}$ samples were incubated with recombinant Src (molar ratio: 5:1) at 30 °C for 1 h. Reactions were quenched by heat-shock (90 °C) and the resultant mixtures were subjected to LC-ESI-TOFMS analysis.

e. Buffer conditions were as follows: 50 mM Tris, pH 7.5, 5 mM $MgCl_2$, 2 mM DTT, 1 mM ATP.

f. Each MTSL addition accounts for an additional 184 daltons.

g. Hyperphosphorylated $PRD^{Strep}_{703-868}$ samples were incubated with MTSL (protein to MTSL molar ratio: 1:10) at room temperature for ~12 h. The excess of unreacted spin label was removed using the HiPrep 26/10 Desalting column (GE Healthcare) and the resultant protein was subjected to LC-ESI-TOFMS analysis.

Table S2. List of search parameters used for LC-MS/MS analyses (see Figs. S3, S4, and S6C)

Search parameters	Name / Entry / Value
Peaklist generating software	MSConvert Proteowizard (version 3.0.21033 64-bit)
Search engine	Knime (version 3.6.0 v201807100937) workflow manager with OpenMS-2.3.0 with MSGFplus adaptor 11/10/2017
Sequence database	Uniprot accession no. Q8WUM4; entry version 197 (02 Jun 2021)
Database entries searched	Only Uniprot accession no. Q8WUM4
Proteases used	PK (non-specific cleavage) and trypsin (cleaves C-terminal to arginine or lysine except when followed by a proline)
Missed / non-specific cleavages permitted	PK: minimum peptide length 6, maximum 60 Trypsin: minimum peptide length 4, maximum 50
Fixed modifications considered	None
Variable modifications considered	PK: phosphotyrosine, deamidated(N) Trypsin: phosphotyrosine, deamidated(N), phosphoserine, phosphothreonine
Mass tolerance for precursor ions	10 parts per million of precursor ion m/z
Mass tolerance for fragment ions	1 m/z
Threshold score/Expectation value	optimized global SpecEValue score ≤ 0.01
False discovery rate	0.05; estimated from OpenMS FalseDiscoveryRate node

SI References.

1. Elias, R. D., Ma, W., Ghirlando, R., Schwieters, C. D., Reddy, V. S., and Deshmukh, L. (2020) Proline-rich domain of human ALIX contains multiple TSG101-UEV interaction sites and forms phosphorylation-mediated reversible amyloids. *Proc. Natl. Acad. Sci. U. S. A.* **117**, 24274-24284
2. Roepstorff, P., and Fohlman, J. (1984) Proposal for a common nomenclature for sequence ions in mass spectra of peptides. *Biomed. Mass Spectrom.* **11**, 601
3. Brademan, D. R., Riley, N. M., Kwiecien, N. W., and Coon, J. J. (2019) Interactive peptide spectral annotator: a versatile web-based tool for proteomic applications. *Mol. Cell. Proteomics* **18**, S193-S201
4. Zhang, Z. Y., Thieme-Sefler, A. M., Maclean, D., McNamara, D. J., Dobrusin, E. M., Sawyer, T. K., and Dixon, J. E. (1993) Substrate specificity of the protein tyrosine phosphatases. *Proc. Natl. Acad. Sci. U. S. A.* **90**, 4446-4450
5. Shen, Y., and Bax, A. (2013) Protein backbone and sidechain torsion angles predicted from NMR chemical shifts using artificial neural networks. *J. Biomol. NMR* **56**, 227-241
6. Sadler, J. B. A., Wenzel, D. M., Williams, L. K., Guindo-Martínez, M., Alam, S. L., Mercader, J. M., Torrents, D., Ullman, K. S., Sundquist, W. I., and Martin-Serrano, J. (2018) A cancer-associated polymorphism in ESCRT-III disrupts the abscission checkpoint and promotes genome instability. *Proc. Natl. Acad. Sci. U. S. A.* **115**, E8900-E8908
7. Clore, G. M., and Iwahara, J. (2009) Theory, practice, and applications of paramagnetic relaxation enhancement for the characterization of transient low-population states of biological macromolecules and their complexes. *Chem. Rev.* **109**, 4108-4139
8. Deshmukh, L., Louis, J. M., Ghirlando, R., and Clore, G. M. (2016) Transient HIV-1 Gag-protease interactions revealed by paramagnetic NMR suggest origins of compensatory drug resistance mutations. *Proc. Natl. Acad. Sci. U. S. A.* **113**, 12456-12461
9. Duan, X., Hall, J. A., Nikaido, H., and Quiocho, F. A. (2001) Crystal structures of the maltodextrin/maltose-binding protein complexed with reduced oligosaccharides: flexibility of tertiary structure and ligand binding. *J. Mol. Biol.* **306**, 1115-1126
10. Ferreira, C. M. H., Pinto, I. S. S., Soares, E. V., and Soares, H. M. V. M. (2015) (Un)suitability of the use of pH buffers in biological, biochemical and environmental studies and their interaction with metal ions – a review. *RSC Adv.* **5**, 30989-31003